

Article

Decentralized Virtual Impedance- Conventional Droop Control for Power Sharing for Inverter-Based Distributed Energy Resources of a Microgrid

Elutunji Buraimoh *, Anuoluwapo O. Aluko, Oluwafemi E. Oni  and Innocent E. Davidson 

Department of Electrical Power Engineering, Durban University of Technology, Durban 4001, South Africa; alukoanuoluwapotobi@gmail.com (A.O.A.); oluwafemio1@dut.ac.za (O.E.O.); innocentd@dut.ac.za (I.E.D.)

* Correspondence: elutunjib@dut.ac.za; Tel.: +27-(0)-73-992-0100

Abstract: The work presents the power-sharing in a standalone low voltage AC microgrid consisting of three parallel grid supporting inverters using a virtual impedance-based droop system. Typically, isolated microgrids suffer unique challenges regarding voltage, current, frequency regulation, power flow control, and power-sharing due to the absence of a stiff AC grid source. This work investigated the power flow and sharing technical challenges using three inverter-based distributed energy sources, three static loads, and one dynamic load. These distributed energy sources are interconnected with the loads using low voltage line impedance within the microgrid to implement the uneven power distribution. Furthermore, a distributed grid supporting control utilizing virtual impedance is proposed in this work to improve power-sharing. The microgrid model is developed with the MATLAB Simulink environment and validated using the Opal RT OP4510 simulator. The proposed technique ensured improved power-sharing and mitigated the effect of voltage drops introduced through a virtual impedance using combined positive and negative virtual.

Keywords: droop control; microgrid; distributed energy resources; virtual impedance



Citation: Buraimoh, E.; Aluko, A.O.; Oni, O.E.; Davidson, I.E.

Decentralized Virtual Impedance- Conventional Droop Control for Power Sharing for Inverter-Based Distributed Energy Resources of a Microgrid. *Energies* **2022**, *15*, 0. <https://doi.org/>

Academic Editor: King Jet Tseng

Received: 28 April 2022

Accepted: 14 June 2022

Published: 16 June 2022

Publisher's Note: MDPI stays neutral with regard to jurisdictional claims in published maps and institutional affiliations.



Copyright: © 2022 by the authors. Licensee MDPI, Basel, Switzerland. This article is an open access article distributed under the terms and conditions of the Creative Commons Attribution (CC BY) license (<https://creativecommons.org/licenses/by/4.0/>).

1. Introduction

A rise in the utilization of small-scale energy generating units is predicted to boost global energy capacity and successfully integrate renewables into the electricity grid system. These are distributed at different locations in the power grid, referred to as distributed energy resources (DER) [1]. Using renewable energy sources increases the demand for power electronic interfaces in distributed generating units [2]. The electricity grid faces additional issues due to renewable's intermittent nature. These units can be linked in parallel to boost a grid's power capacity. This poses additional energy supply and stability [3]. The conventional power system is characterized by unidirectional power flows, with massive synchronous generators serving as the primary generation source. In addition, the move toward greater renewable power has resulted in additional elements such as grid-based energy storage devices. Customers are referred to as prosumers because they both use and create energy, resulting in bidirectional power flow [4]. Traditional control strategies based on massive, synchronous generators are not necessarily relevant in the future power grid due to the current development in distributed generation [5]. New control approaches must be designed to handle the new problems while also considering the benefits of emerging technology and generating units with power electronic interfaces.

Microgrid provides a veritable platform to address the issues of integrating renewables by providing a mini version of a power system that includes distributed generation and energy storage. A microgrid is a system with well-defined electrical borders, local control systems, and flexible loads [6]. Microgrids are beneficial for integrating distributed generation, ensuring reliable power supply, and addressing difficulties such as bidirectional power flows, prosumers, and intermittent production [7]. Microgrids can be electrically

linked to the main grid or run independently. The latter method of operation, known as “island mode”, necessitates some kind of energy storage and local control mechanism. Controlling power flow, voltage, and frequency is critical in the island mode of operation. Each generation unit possesses a local control system in charge of the microgrid’s voltage and frequency levels. This mode of operation can help ensure power delivery in an unintentional disconnect from the main grid [8]. In addition, microgrids safeguard electricity in unconnected remote regions [9]. The main grid recognizes the microgrid as a single entity and stabilizes its voltage level when grid-connected; therefore, its control requirement is to deliver power to the main grids [10].

A centralized or decentralized control strategy operates a microgrid’s local control system. The control systems at the DER units follow directions from the microgrid’s central controller in a centralized fashion [11]. The central controller can control the different units concerning each other using this method. The microgrid’s power flow regulation and safe operation are simplified as compared to a decentralized method [12]. However, the centralized model has its drawbacks, such as the significant expenses associated with the necessity for communication [13]. Because the centralized controller is intended for a specific microgrid, it becomes more difficult to expand the microgrid with more units or in the event of a DG failure [14]. Because the microgrid is reliant on the centralized controller, a breakdown in the control or communication can bring the entire microgrid to a halt. Unlike the centralized method, a decentralized microgrid features more intelligent controllers installed at the DG units [1]. Because the control is done locally, extra complications are associated with the interaction between the DER units, including power flow concerns [9]. This control strategy is more efficient for DER failure or microgrid expansions since it uses local metrics. Because of these benefits, the decentralized control technique is of great interest. This technique allows for more generic research because the controllers are not dependent on a specific microgrid system. Even while decentralized controllers are less reliant on communication, it is essential to note that they are not entirely devoid of it. The communication is linked to the upper levels of control, which work at a slower sample rate. As a result, the implications of communication failures will be less severe than in the case of a centralized controller.

Using the specified droop control algorithms for a decentralized control method is straightforward when using local voltage and frequency data. However, when it comes to power-sharing, the issues posed by output impedance variances are inherent. For example, the conventional and inverse droops have characteristics based on either an entirely inductive or resistive output impedance. On the other hand, the output impedance of a real microgrid is made up of both resistance and reactance. As a result, active and reactive power are coupled, dependent on voltage and frequency levels [15]. Various challenges occur when traditional droop control is utilized in systems with resistive or output impedances since the control approach is predicated on exclusively inductive output impedances. As mentioned in [16], traditional droop control can offer stable and useful performance in a system with mostly resistive output impedances. However, when using conventional droop control with mostly resistive output impedances, the stability margins are reduced, and the issues associated with reactive power sharing typically rise [17]. Furthermore, stability concerns might emerge if the control settings are not correctly chosen, especially with local loads and substantial output impedances [18]. The active power has only a minimal impact on the stability issues; however, the reactive droop coefficient and the output resistance are crucial. According to [19], using conventional droop control in a predominantly resistive microgrid results in poor grid-connected power control transient behavior. The problems are significantly more significant in island mode, resulting in worse reactive power-sharing and more stability issues.

Stability issues arise when the opposite droop control is applied to a primarily inductive output impedance. Because of these stability issues and the importance of correct active power dispatch, opposite droop management is rarely utilized in microgrids with primarily inductive output impedances. In addition to the accurate active power-sharing,

the traditional droop control's similar behavior and compatibility with synchronous generators are frequently preferred [References]. Furthermore, the typical droop control can provide virtual inertia to the system by carefully selecting the droop coefficients [20]. In some circumstances, however, the direct voltage control of the opposite droop control is preferred due to the more stable functioning with mostly resistive output impedances [21]. Even though the droop control methods provide unstable responses with specific output impedances, virtual impedances are an excellent way to change the inverters' output impedance. It can generate steady, high-performance responses practically regardless of the inverters' real output impedance [16].

The virtual impedances have been utilized in converter control for harmonic voltage correction and increased stability and power-sharing applications [22]. The values of virtual impedances were researched by [23] to maximize the microgrid's performance. The virtual impedances can assist in keeping the voltage under particular limits, share reactive power effectively, dampen the system, and decouple active and reactive power. A virtual impedance, in general, mimics the behavior of a genuine impedance while avoiding losses. The size of the impedance and the relationship between the resistive and reactive components must be considered in selecting virtual impedances. Ref. [24] provides a detailed analysis of the benefits and drawbacks of using virtual impedance with droop control. The virtual impedances can be utilized to compensate for physical output impedance mismatches between inverters. The fundamental purpose of virtual impedance is to change the impedance angle of the corresponding output impedance. Positive inductive- or negative resistive virtual impedances can be introduced to low-voltage grids to provide inductive equivalent output impedance for inverters using standard droop control. Furthermore, this may help to increase the stability margins. Power-sharing is greatly improved with existing virtual impedance solutions. The voltage losses associated with these systems, on the other hand, can be rather substantial [25].

Thus, this paper proposes a virtual impedance solution that can decrease voltage drops with a design that divides one virtual impedance into two components. These components consist of the virtual voltage drop across the virtual resistance and impedance like a typical physical impedance with the cross-decoupling components from the direct and quadrature components of the output current. This addresses the output impedance matching. Thus, the voltage loss through the virtual impedances is mitigated. The virtual impedances are implemented alongside the traditional droop control. The decoupling of active and reactive power is more substantial with this method than with inductive virtual impedances alone. Furthermore, voltage dips across virtual impedances are minimized. The work presents the power-sharing in a standalone low voltage AC microgrid consisting of three parallel grid supporting inverters using a virtual impedance-based droop system. This work investigated the power flow and sharing technical challenges using three inverter-based DERs, three static loads, and one dynamic load. These DERs are interconnected with the loads using low voltage line impedance within the microgrid to implement the uneven power distribution. The microgrid model is developed with the MATLAB Simulink environment and validated using the Opal RT OP4510 simulator. The proposed technique ensured improved power-sharing and mitigated the effect of voltage drops introduced through a virtual impedance.

2. System Control

Droop control uses conventional or inverse droop control, using the relationship between the voltage and frequency in the grid and the power produced by the inverters without the requirement for communication between inverters [26]. The frequency and voltage levels indicate power generations in a microgrid, and the droop utilizes this information in modifying the power delivered by the inverters using active and reactive power setpoints. This technique makes grid expansion provisions to accommodate more DERs and dispersed loads. The provision for disconnection of DERs and loads is also allowed. In

addition, droop control does not need high-speed communication; thus, it considerably saves costs with exemplary dependability [27].

2.1. Droop Control

Typical low-voltage microgrids and networks have resistive line impedances; however, point of common coupling (PCC) transformers and LC or LCL filters contribute to their inductive behavior. Thus, the output impedance might become primarily inductive in the event of insignificant line impedances. The traditional droop control regulates power-sharing with inductive output impedances. Equations (1) and (2) for both active and reactive powers, in line with two other crucial assumptions, serve as the foundation for the development of this method [23]:

$$P = \frac{V_1^2}{Z} [\cos \theta] - \frac{V_1 V_2}{Z} [\cos(\theta + \delta)] \quad (1)$$

$$Q = \frac{V_1^2}{Z} [\sin \theta] - \frac{V_1 V_2}{Z} [\sin(\theta + \delta)] \quad (2)$$

The output impedance is assumed to be entirely inductive; the impedance Z is equivalent to only reactance, X . Thus, the impedance angle θ equals 90. The assumption that the power angle is minimal is based on an insignificant phase difference between the voltage at the inverter's output and the voltage at the loads' connection point. Thus, the power angle and the voltage drop across output impedance are given by Equations (3) and (4) [28]. Therefore, the active power relies on the power angle directly relating to the frequency. Similarly, the voltage drop, $V_1 - V_2$, is proportional to the reactive power. These are represented as Equations (5) and (6), indicating that conventional droop is dependent on a rated voltage E^* and frequency ω^* [19].

$$\delta \approx \frac{PX}{V_1 V_2} \quad (3)$$

$$V_1 - V_2 \approx \frac{QX}{V_1} \quad (4)$$

$$P^* - P = \frac{1}{k_P} [\omega - \omega^*] \quad (5)$$

$$Q^* - Q = \frac{1}{k_Q} [E - E^*] \quad (6)$$

where P , Q , E , and ω , are the observed values of the active power, reactive power voltage, and frequency, respectively. k_P and k_Q are the active and reactive droop coefficients, respectively, governing the relationship between frequency and active power and voltage and reactive power. The active power provided into the line is regulated by frequency fluctuations, while voltage deviations control the reactive power supply [29]. The droop coefficients determine the deviations; k_P is the maximum allowable frequency deviation ratio owing to a change in active power due to a load change, while k_Q is the ratio of the maximum permissible voltage change related to a load change in reactive power. The maximum deviations permitted in the grid are frequently used to determine the ratios [24]. k_P and k_Q impact inverter power-sharing, with more significant values resulting in improved power-sharing. Nevertheless, the coefficients have limitations beyond which further increment results in system instability [19]. Droop coefficient selection within the stability constraints is a trade-off between power-sharing performance and voltage and frequency aberrations. In a microgrid, the droop coefficients of two DERs must be the same to share the same amount of power.

The conventional technique is an efficient strategy to regulate frequency and voltage relative to the generated power when output impedances are purely inductive. Active power is distributed evenly among inverters; however, this technique has several limitations

regarding reactive power distribution. Unequal reactive power supply from inverters is frequently caused by a discrepancy in output voltage or output impedances, occurring with distribution lines of differing lengths [11]. Thus, reactive circulation currents are created as a result, while purely inductive distribution lines result in an unstable response [30].

$$P = \frac{3}{2}(v_d i_d + v_q i_q) \quad (7)$$

$$Q = \frac{3}{2}(v_q i_d - v_d i_q) \quad (8)$$

The measured values of active power P and reactive power Q are calculated from the direct-axis component of the voltage and current, v_d and i_d , and the quadrature-axis component of the voltage and current, v_q and i_q , using Equations (7) and (8). Only v_d is connected to the droop characteristic, as this is equivalent to E , while v_q is constrained to zero. Low-pass filters (LPF) filter P and Q to alleviate the impact of high-frequency components in the droop and ensure a suitable bandwidth difference between the inner loops and the droop [9]. However, this causes the droop controller to run slowly, reducing the power-sharing performance. The droop controller's output frequency ω is integrated, resulting in a continually changing angle, ωt employed in Clark's transformation to align voltage vectors at the output of the inverters in the synchronous reference frame.

The droop characteristic based on the assumption of entirely resistive output impedances is invalid, considering resistive components dominate output impedances in low-voltage microgrids [11]. The reactive power determines the power angle and frequency, whereas the active power determines the voltage drop [31]. Like in traditional droop control, the droop coefficients are selected based on active and reactive power changes and maximum voltage and frequency deviations associated with these changes. The reverse droop control outperforms the traditional droop control for direct voltage control and harmonic power-sharing. The system is more damped, and phase mistakes have less impact on active power-sharing. Conventional droop control is more widely utilized due to improved active power-sharing [11].

2.2. Complex Virtual Impedance Technique

The virtual impedance is presented as a control technique in conjunction with droop control for power control and power-sharing. Similarly, virtual impedances are utilized in converter control for applications such as harmonic voltage correction and increased stability and power-sharing [22]. Because of its numerous applications, the value of this impedance must be determined according to its intended function. The values of virtual impedances are researched in [23] in order to maximize the microgrid's performance. The virtual impedances aid the regulation of the voltage under particular limits, share reactive power effectively, dampen the system, and decouple active and reactive power. A virtual impedance, in general, mimics the behavior of a normal impedance while avoiding losses [22]. In the existing (typical) technique, the virtual impedance is selected to make the 'equivalent' output impedance rather than resistance and reactance. This achieves improved active and reactive power decoupling and accurate power-sharing.

Equation (9) represents the general architecture for virtual impedance loops with the grid alternating current I_{abc} and the virtual impedance, Z_o ; both affect the inner loop control's voltage reference V^* and constitute virtual impedance voltage drop ΔV_o . Thus, ΔV_o is subtracted from a droop control voltage drop V^{**} to determine the voltage reference of the inner loop. This adjusts the equivalent output impedance's magnitude and impedance angle. As given in Equation (9), using virtual impedances has the drawback of lowering the voltage reference; thus, this must be considered when determining the impedance value. Equation (9) is implemented in the synchronous reference frame for the d and q axis in the inner loop, as shown in Equation (10)

$$V^* = V^{**} - \Delta V_o = V^{**} - Z_o I_{abc} \quad (9)$$

$$\begin{aligned} V_d^* &= V_d^{**} - R_o i_d - X_o i_q \\ V_q^* &= V_q^{**} - R_o i_q - X_o i_d \end{aligned} \quad (10)$$

With droop control algorithms, virtual impedances are utilized to optimize active and reactive power-sharing by compensating for physical output impedance mismatches between inverters. This strategy is successful in active and reactive power-sharing, provided the participating parallel inverters have the same equivalent output impedance. Therefore, the virtual impedance is chosen to ensure that the equivalent output (physical and virtual) impedance for all inverters in the system is equal. The fundamental purpose of virtual impedance is to change the impedance angle of the corresponding output impedance. In addition, a negative resistance and positive reactance constitute inductive virtual impedances, as shown in Equation (9), thereby increasing the stability margins [32].

A similar method may be used for the opposite droop control approach, but the virtual impedance has a substantial resistive value. When virtual impedances are employed to make corresponding output impedances more inductive or resistive, the virtual impedances' size is usually chosen to dominate the physical output impedances [33]. This guarantees that the active and reactive power are appropriately decoupled. The relative difference between the equivalent output impedance is lowered when the physical output impedances of the inverters are uneven, which benefits power-sharing [34]. The resistive virtual impedances contribute to more excellent system damping and better power-sharing.

Power-sharing is greatly improved with existing virtual impedance solutions. The voltage losses associated with these systems, on the other hand, can be rather substantial [35]. Thus, this work proposes virtual impedance solutions that decrease voltage drops. The virtual impedance design divides one virtual impedance into three components to ensure output impedance matching, as shown in Equation (11). The resistive-inductive virtual impedances, with the virtual voltage drop expressed for synchronous reference frame implementation, is shown in Equation (12). The v_{dpd} and v_{dpq} drop in voltage is due to the virtual impedance

$$v_{dp-abc} = Ri_{abc} + L \frac{di_{abc}}{dt} \quad (11)$$

$$\begin{aligned} v_{dpd} &= Ri_d - \omega Li_q + L \frac{di_d}{dt} \\ v_{dpq} &= Ri_q - \omega Li_d + L \frac{di_q}{dt} \end{aligned} \quad (12)$$

To make the equivalent output impedance of all parallel equal, this arrangement ensures that virtual impedance is applied to the inverter with the lower physical output impedance when there is a sudden increase in load. The total voltage loss through the virtual impedances is greatly minimized with the application of virtual impedances in all parallel inverters. A negative virtual impedance is introduced to the inverter with the higher physical output impedance, and a positive virtual impedance is added to the inverter with the lower physical output impedance to match the output impedances. Thus, different levels of voltage drops are observed across each inverter. Similarly, the location of load increase is varied within the microgrid at points A, B, and C to observe the power-sharing and voltage across each inverter's virtual impedances.

Low pass filters (LPFs) are employed to create a voltage level that is less impacted by high-frequency oscillations due to the derivative term in these virtual impedance loops. Because derivative terms and high-frequency current components can generate considerable voltage deviations, the filters help maintain the voltage dips induced by virtual impedance within tolerable ranges. Figure 1 shows inverter control with virtual impedance and conventional droop. Figure 2 depicts the virtual impedance implementation utilized in this study, including the low-pass filters. LPFs have the problem of causing a phase shift, thereby modifying the behavior of the virtual impedance. LPFs also add an extra-temporal delay to the system, resulting in a significantly slower dynamic response. Therefore, the

cut-off frequency ω_c of the low-pass filters employed in the virtual impedance is equal to the frequency of the system's third harmonic oscillations, as given in Equation (13).

$$\begin{aligned} v_{dpd} &= Ri_d - \omega Li_q + \frac{\omega_c}{s+\omega_c} sLi_d \\ v_{dpq} &= Ri_q - \omega Li_d + \frac{\omega_c}{s+\omega_c} sLi_q \end{aligned} \tag{13}$$

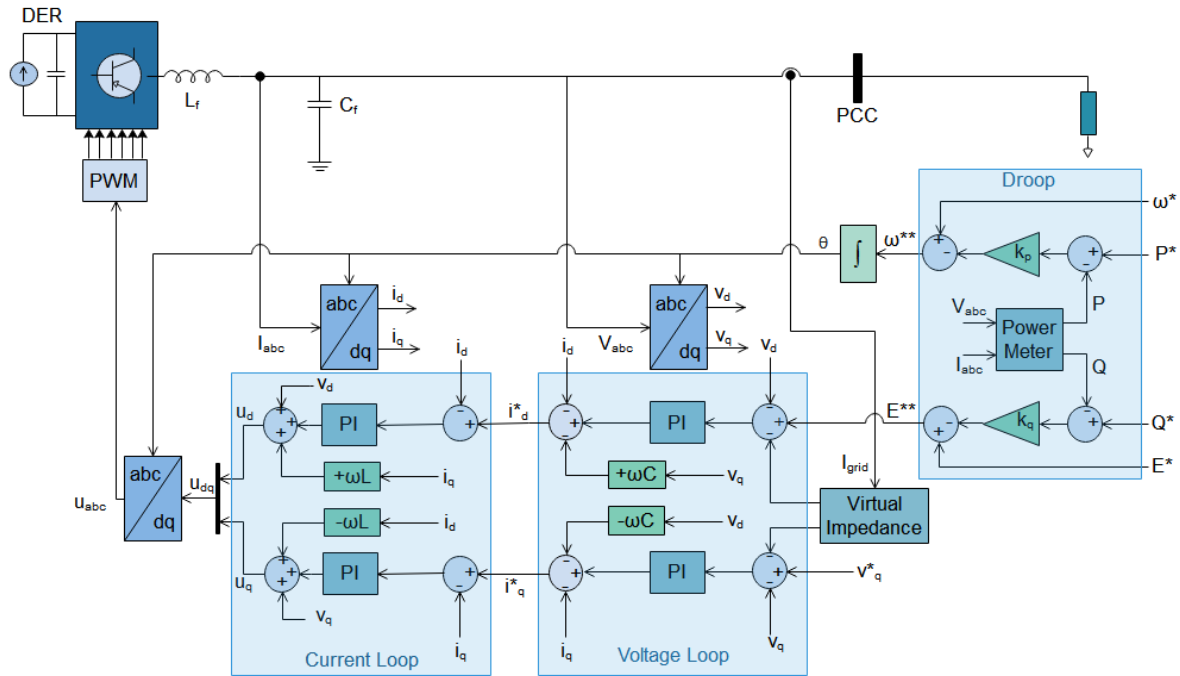


Figure 1. Inverter control with virtual impedance and conventional droop.

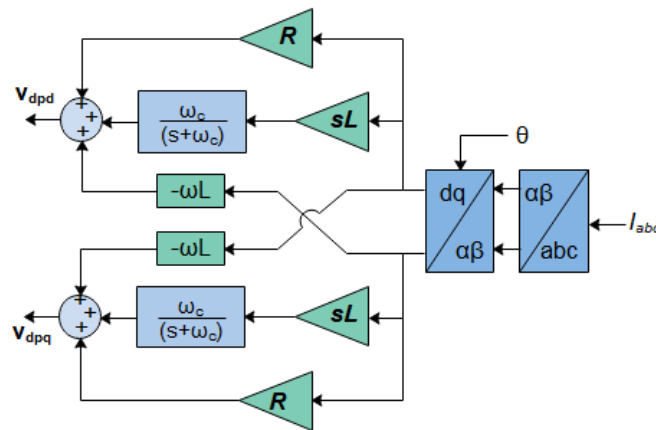


Figure 2. Proposed Virtual Impedance Model.

Therefore, the virtual impedance is realized by subtracting Equation (13) from the preferred reference of voltage as indicated in Equation (14). Equations (14) and (15) implement external voltage control and internal current control for each inverter, as shown in Figure 1.

$$\begin{aligned} i_d^* &= i_d - (\omega C_f)v_q + \left(k_{pv} + \frac{k_{iv}}{s}\right) [v_d^* - v_d - v_{dp-d}] \\ i_q^* &= i_q + (\omega C_f)v_d + \left(k_{pv} + \frac{k_{iv}}{s}\right) [v_q^* - v_q - v_{dp-q}] \end{aligned} \tag{14}$$

$$\begin{aligned} u_d &= v_d - (\omega L_f)i_q + \left(k_{pi} + \frac{k_{ii}}{s}\right) [i_d^* - i_d] \\ u_q &= v_q + (\omega L_f)i_d + \left(k_{pi} + \frac{k_{ii}}{s}\right) [i_q^* - i_q] \end{aligned} \tag{15}$$

where k_{IV} and k_{PV} are the integral gain and proportional gain of the voltage PI control, respectively. Where k_{ii} and k_{pi} indicate integral and proportional gains, respectively, from the current control loop. The v_d and v_q elements of the voltage direct-quadrature axes imply feed-forward quantities. Feed-forward and cross decoupled quantities are used to perform independent controls of the current dq axis.

This control loop regulates the active and reactive power to ensure power transfer from DC to the inverter's AC side. The voltage v_d is constant, and the active power is regulated by adjusting the current i_d . Similarly, the reactive power is regulated through the current i_q control. The grid-supporting systems' inner loop controls the filter inductor current, following current references and removing cross-coupled terms caused by the reference frame transformation. The entire system reference is the standard frame where each constituent generating unit's dynamics are transformed using the angular frequency ω . Subsequently, the decoupling of the active and reactive power is done through Park transformation ($abc - dq$).

3. Results

The isolated microgrid consists of three inverter-based distributed energy sources, which are given in Figure 3. The microgrid model consists of three loads connected while the fourth load is connected at a time of $t = 1.5$ s to investigate the power-sharing using a typical virtual impedance given in Equation (10) and the proposed virtual impedance given in Equation (12). These virtual impedance models are utilized alongside the conventional droop technique.

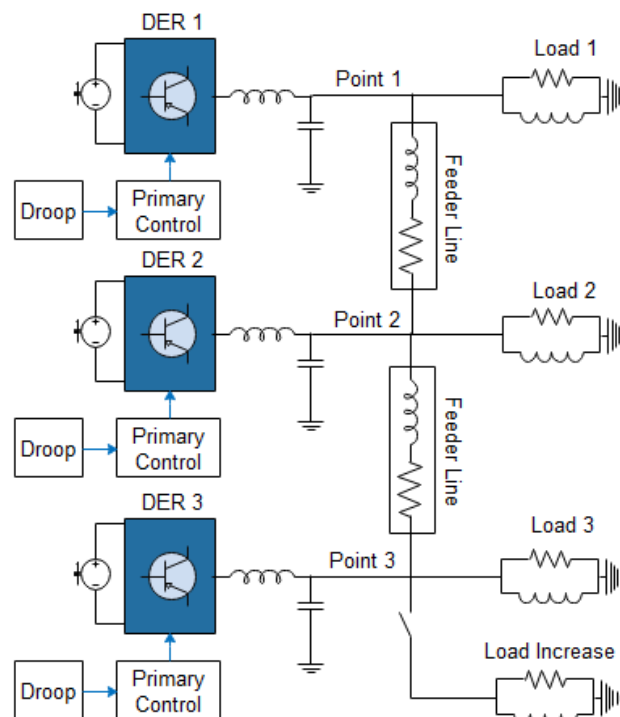


Figure 3. Investigated Decentralized Islanded Microgrid.

The virtual impedance is presented as a control technique in conjunction with droop control for power control and power-sharing. Similarly, virtual impedances are utilized in converter control for applications such as harmonic voltage correction and increased stability and power-sharing. The virtual impedances keep the voltage under limits, share reactive power effectively, dampen the system, and decouple active and reactive power. The presented virtual impedance mimicked the behavior of a typical impedance while avoiding losses. The voltage drop across typical virtual impedance and proposed impedance is given in Figures 4–7 for both the d-axis and the d-axis voltage drop across the impedances. The

increased voltage drop at the output of DER 3 is due to the proximity and operation of the switch that connects the load increase.

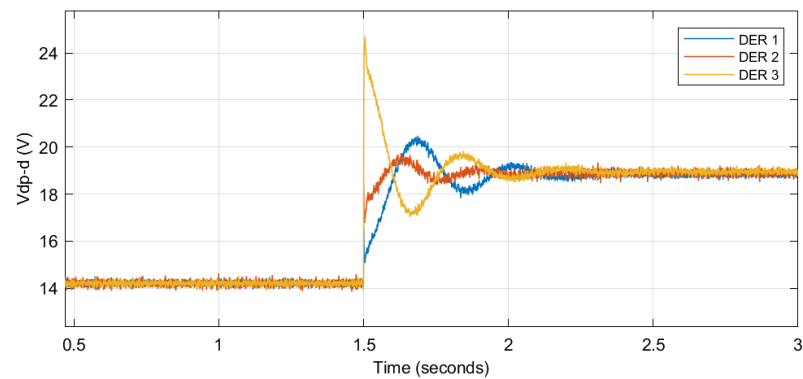


Figure 4. v_{dpd} drop in voltage due to typical virtual impedance.

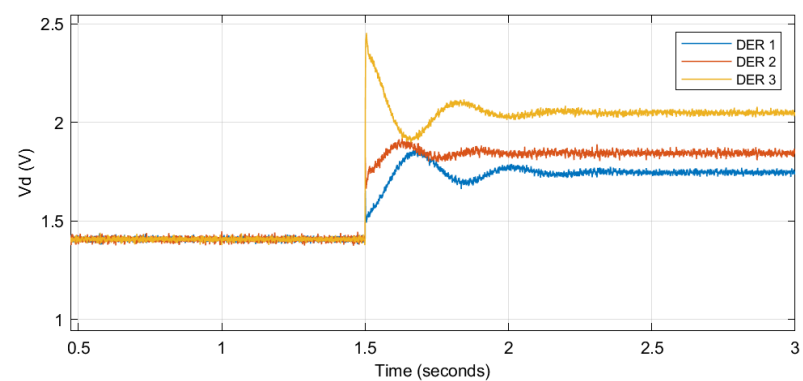


Figure 5. v_{dpd} drop in voltage due to proposed virtual impedance.

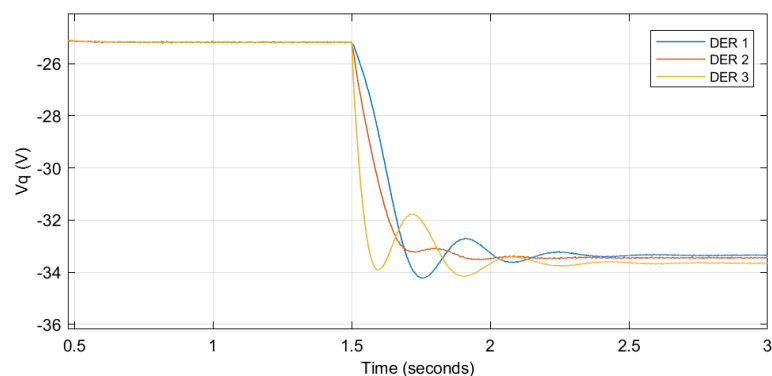


Figure 6. v_{dpq} drop in voltage due to typical virtual impedance.

The isolated microgrid system provided in this work utilized virtual impedance and conventional droop to investigate power-sharing problems in microgrids. The virtual impedance affected both affect the d and q voltage reference. The voltage reference from the droop control is subtracted from a voltage drop generated by the virtual impedance to give the reference to the inner control loops. Ordinarily, the typical virtual impedance adjusts the equivalent output impedance's magnitude and impedance angle, thus, lowering the voltage reference and the output AC voltage. However, the proposed method can regulate the output voltage with an insignificant drop in droop voltage and AC output voltage in Figures 8 and 9, respectively. The corresponding AC output voltages observed for the three DERs are given in Figure 10.

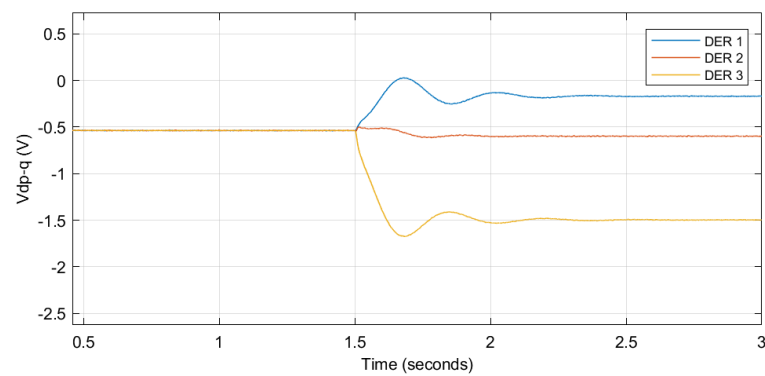


Figure 7. v_{dpq} drop in voltage due to proposed virtual impedance.

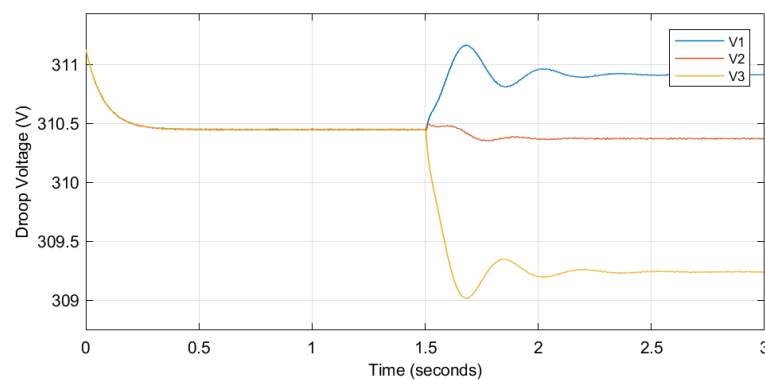


Figure 8. Output voltage reference of the droop controller with typical virtual impedance.

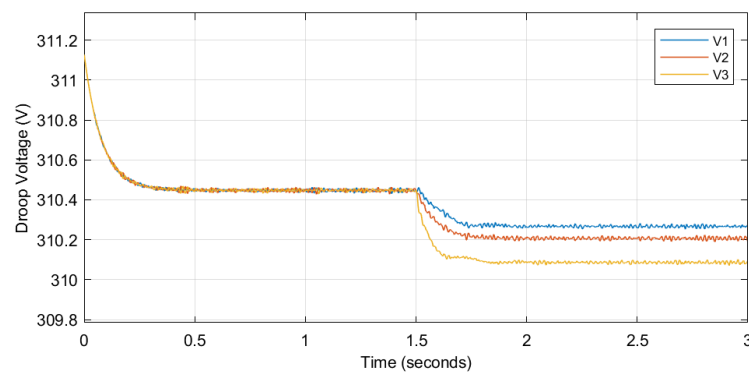


Figure 9. Output voltage reference of the droop controller with proposed virtual impedance.

This virtual impedance proposed mitigated the voltage's negative impacts by introducing combined positive and negative virtual impedances. The voltage reference from the droop controller is given in Figures 8 and 9, and the voltage drop owing to the virtual impedance is insignificant in output voltage in Figure 10 for the proposed virtual impedance. The virtual impedances compensated the physical output impedance mismatches between inverters, ensuring active and reactive power-sharing, as given in Figures 11 and 12.

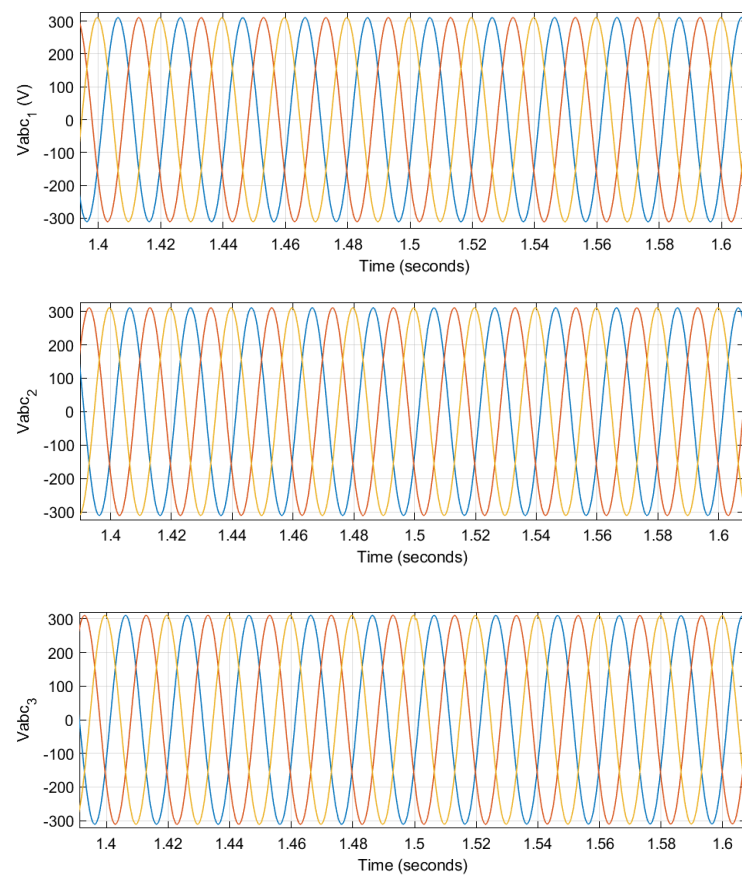


Figure 10. Three-phase AC output voltage of three DERs with proposed virtual impedance.

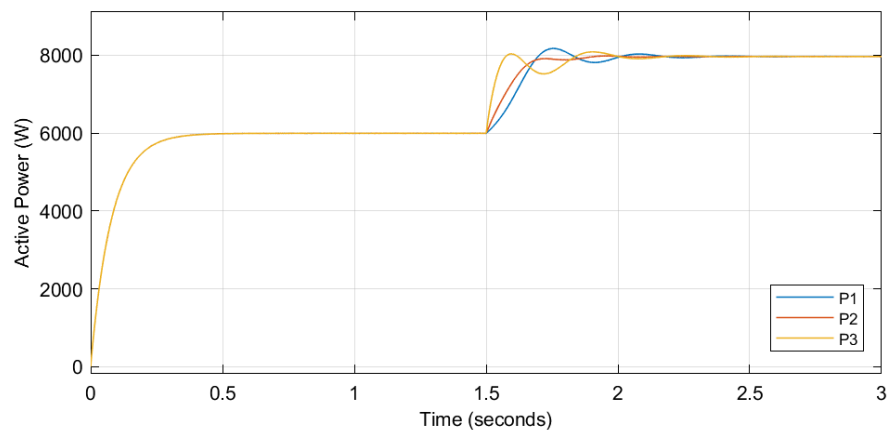


Figure 11. Active power output of the droop controller with typical virtual impedance.

Figure 13 indicates that an unequal reactive power supply from inverters is frequently caused by a discrepancy in output voltage or output impedances, occurring with distribution lines of differing lengths. Thus, reactive circulation currents are created, while purely inductive distribution lines result in an unstable response. The proposed virtual impedance reduces circulating currents, even with both resistive and inductive components in the distribution lines. Thus, the drawback of conventional droop is overcome by the proposed virtual impedance with the relatively improved reactive power-sharing in Figure 14. The single-phase current outputs of all the three DERs are given in Figure 15.

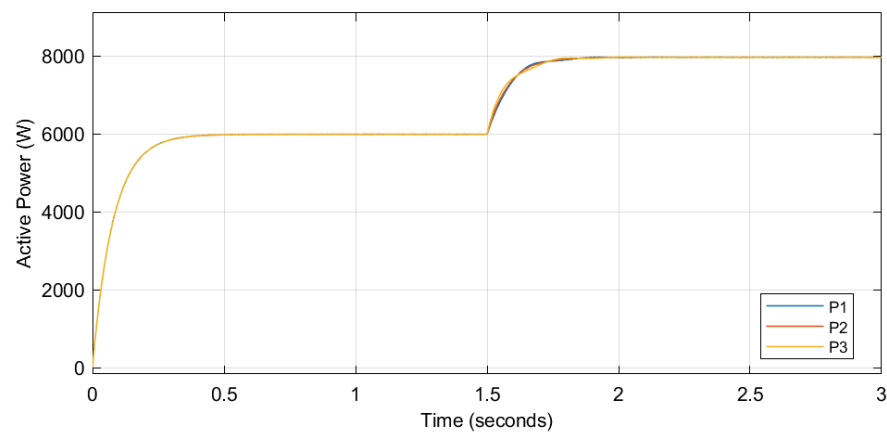


Figure 12. Active power output of the droop controller with proposed virtual impedance.

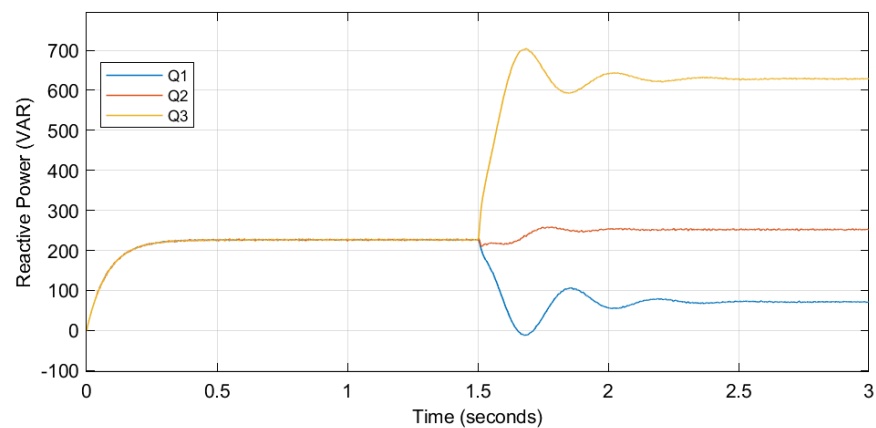


Figure 13. Reactive power output of the droop controller with typical virtual impedance.

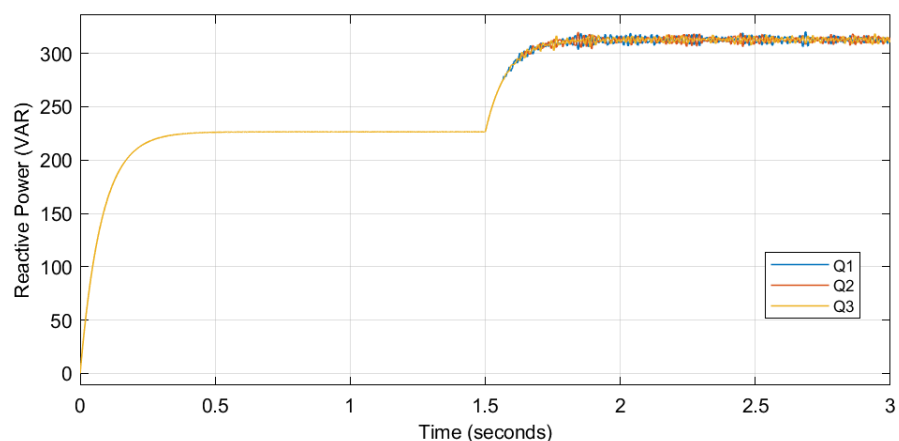


Figure 14. Reactive power output of the droop controller with proposed virtual impedance.

Power-sharing is greatly improved with the proposed virtual impedance solutions with decreased voltage drops. Furthermore, the voltage loss through the virtual impedances is minimized with virtual impedances introduced into the droop of each inverter. As indicated, the virtual impedance voltage output was introduced to the outer loop, which considerably minimized the voltage drop caused by the usage of conventional virtual impedances.

Typical virtual impedances create a substantial voltage loss due to their size, while the proposed approach mitigates this voltage drop. An exceptional and precise synchronization scheme is used for parallel operation with other inverters, as shown in Figures 16 and 17. The output impedances of each inverter determine their respective power-sharing when

operated in parallel. The system operates steadily in island mode with operating conditions within the specified technical limit. The microgrid stipulates and regulates the supply voltage and frequency to the AC loads.

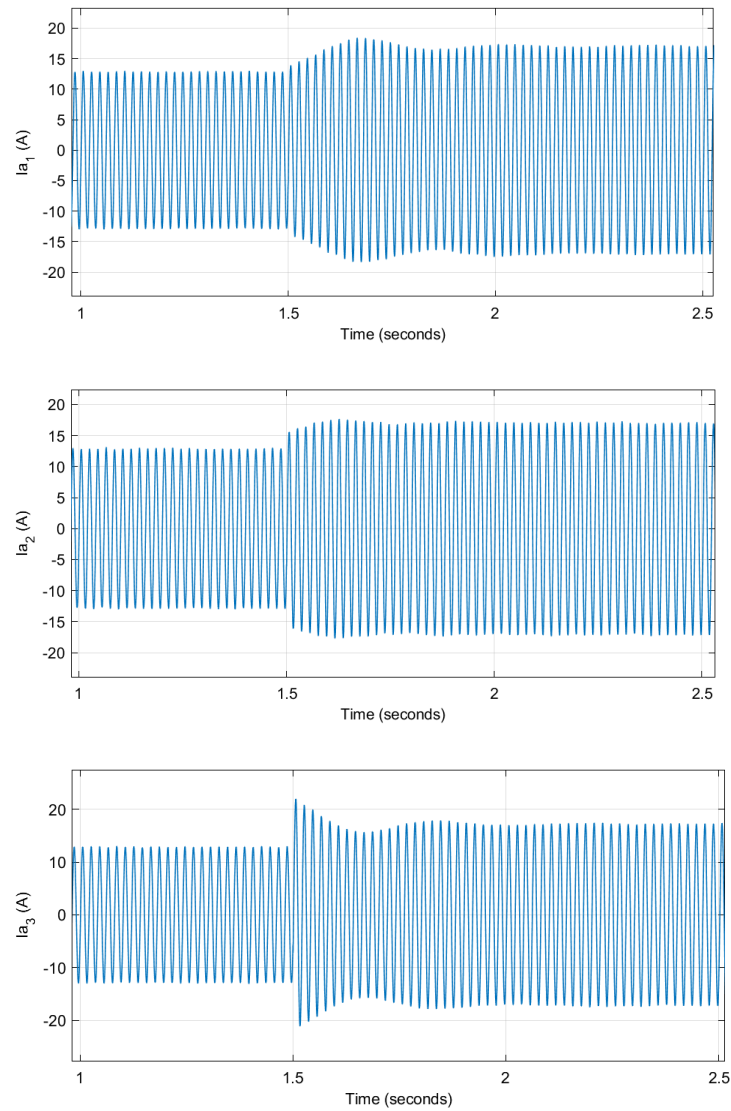


Figure 15. Single-phase AC output currents of three DERs with proposed virtual impedance.

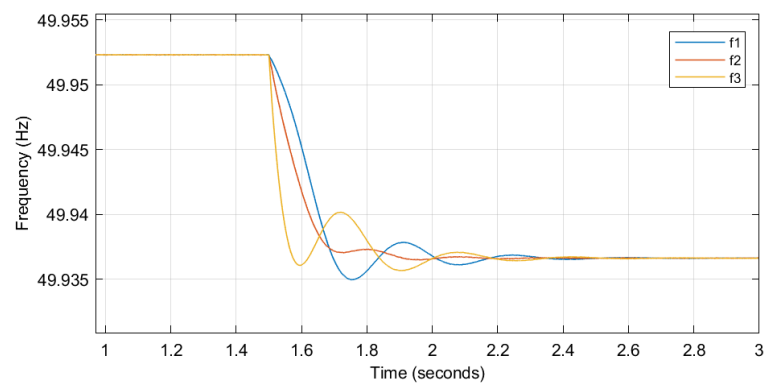


Figure 16. Frequency output of the droop controller with typical virtual impedance.

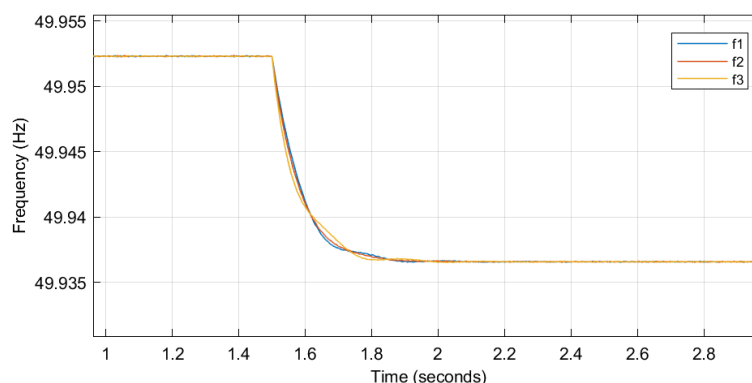


Figure 17. Frequency output of the droop controller with proposed virtual impedance.

4. Conclusions

Using a design that separates one virtual impedance into two components, this study provides a virtual impedance solution that can reduce voltage drops. The virtual voltage drop across the virtual resistance and impedance, similar to a typical physical impedance, with the cross decoupling components from the direct and quadrature components of the output current, makes up these components. As a result, the output impedance matching and the voltage loss due to virtual impedances are reduced. The virtual impedances are used in conjunction with conventional droop control. This approach decouples active and reactive power more effectively than inductive virtual impedances alone. Voltage dips across virtual impedances are also kept to a minimum. The paper shows how a virtual impedance-based droop system may be used to share power in a standalone low voltage AC microgrid with three parallel grid supporting inverters. These DERs are coupled with the loads inside the microgrid utilizing low voltage line impedance to execute the unequal power distribution. The suggested method increased power-sharing and reduced the impact of voltage drops generated by a virtual impedance. The proposed technique is recommended for loads drawing in currents in abrupt short pulses, such as non-linear loads, for future work. These pulses distort the current waveforms, generating harmonics that can lead to power problems affecting the microgrid and the other local loads.

Author Contributions: Conceptualization, E.B., I.E.D., A.O.A. and O.E.O.; methodology, E.B., I.E.D., A.O.A. and O.E.O.; software, E.B. and A.O.A.; validation, E.B., I.E.D., A.O.A. and O.E.O.; formal analysis, E.B., I.E.D., A.O.A. and O.E.O.; investigation, E.B., I.E.D., A.O.A. and O.E.O.; resources, I.E.D.; data curation, E.B.; writing—original draft preparation, E.B., I.E.D., A.O.A. and O.E.O.; writing—review and editing, E.B.; visualization, E.B.; supervision, I.E.D.; project administration, E.B.; funding acquisition, I.E.D. All authors have read and agreed to the published version of the manuscript.

Funding: The APC was funded by DUT Smart Grids Research and DUT Directorate for Research and Postgraduate Supports.

Data Availability Statement: Not applicable.

Acknowledgments: We acknowledge the support given by DUT Smart Grids Research and DUT Directorate for Research and Postgraduate Supports.

Conflicts of Interest: The authors declare no conflict of interest.

References

1. Mokhtar, M.; Marei, M.I.; El-Sattar, A.A. An Adaptive Droop Control Scheme for DC Microgrids Integrating Sliding Mode Voltage and Current Controlled Boost Converters. *IEEE Trans. Smart Grid* **2019**, *10*, 1685–1693. [[CrossRef](#)]
2. Liu, J.; Miura, Y.; Ise, T. Comparison of Dynamic Characteristics between Virtual Synchronous Generator and Droop Control in Inverter-Based Distributed Generators. *IEEE Trans. Power Electron.* **2016**, *31*, 3600–3611. [[CrossRef](#)]
3. Hagh, M.T.; Khalili, T. A Review of Fault Ride-Through of PV and Wind Renewable Energies in Grid Codes. *Int. J. Energy Res.* **2018**, *43*, 1342–1356. [[CrossRef](#)]

4. Zhang, R.; Hredzak, B. Distributed Dynamic Clustering Algorithm for Formation of Heterogeneous Virtual Power Plants Based on Power Requirements. *IEEE Trans. Smart Grid* **2021**, *12*, 192–204. [[CrossRef](#)]
5. Shi, K.; Song, W.; Ge, H.; Xu, P.; Yang, Y.; Blaabjerg, F. Transient Analysis of Microgrids with Parallel Synchronous Generators and Virtual Synchronous Generators. *IEEE Trans. Energy Convers.* **2020**, *35*, 95–105. [[CrossRef](#)]
6. Zuo, S.; Altun, T.; Lewis, F.L.; Davoudi, A. Distributed Resilient Secondary Control of DC Microgrids against Unbounded Attacks. *IEEE Trans. Smart Grid* **2020**, *11*, 3850–3859. [[CrossRef](#)]
7. Cheng, Y.; Qian, C.; Crow, M.L.; Pekarek, S.; Atcitty, S. A Comparison of Diode-Clamped and Cascaded Multilevel Converters for a STATCOM with Energy Storage. *IEEE Trans. Ind. Electron.* **2006**, *53*, 1512–1521. [[CrossRef](#)]
8. Buraimoh, E.; Davidson, I.E.; Martinez-Rodrigo, F. Fault Ride-through Enhancement of Grid Supporting Inverter-Based Microgrid Using Delayed Signal Cancellation Algorithm Secondary Control. *Energies* **2019**, *12*, 3994. [[CrossRef](#)]
9. Deng, Y.; Tao, Y.; Chen, G.; Li, G.; He, X. Enhanced Power Flow Control for Grid-Connected Droop-Controlled Inverters with Improved Stability. *IEEE Trans. Ind. Electron.* **2017**, *64*, 5919–5929. [[CrossRef](#)]
10. Naderi, M.; Khayat, Y.; Shafiee, Q.; Dragicevic, T.; Bevrani, H.; Blaabjerg, F. Interconnected Autonomous AC Microgrids via Back-to-Back Converters-Part II: Stability Analysis. *IEEE Trans. Power Electron.* **2020**, *35*, 11801–11812. [[CrossRef](#)]
11. He, J.; Liu, Y.; Wang, Y. Cascaded Droop and Inverse Droop Regulation for Two-Layer Coordinated Power Flow Control in Series-Connected Power Cells. *IEEE Trans. Ind. Electron.* **2021**, *68*, 6939–6951. [[CrossRef](#)]
12. Yang, H.; Yi, D.; Zhao, J.; Dong, Z. Distributed Optimal Dispatch of Virtual Power Plant via Limited Communication. *IEEE Trans. Power Syst.* **2013**, *28*, 3511–3512. [[CrossRef](#)]
13. Diaz, N.L.; Dragicevic, T.; Vasquez, J.C.; Guerrero, J.M. Intelligent Distributed Generation and Storage Units for DC Microgrids—A New Concept on Cooperative Control without Communications beyond Droop Control. *IEEE Trans. Smart Grid* **2014**, *5*, 2476–2485. [[CrossRef](#)]
14. Lee, W.G.; Nguyen, T.T.; Yoo, H.J.; Kim, H.M. Low-Voltage Ride-through Operation of Grid-Connected Microgrid Using Consensus-Based Distributed Control. *Energies* **2018**, *11*, 2867. [[CrossRef](#)]
15. Rajesh, K.S.; Dash, S.S.; Rajagopal, R.; Sridhar, R. A Review on Control of AC Microgrid. *Renew. Sustain. Energy Rev.* **2017**, *71*, 814–819. [[CrossRef](#)]
16. Tayab, U.B.; bin Roslan, M.A.; Hwai, L.J.; Kashif, M. A Review of Droop Control Techniques for Microgrid. *Renew. Sustain. Energy Rev.* **2017**, *76*, 717–727. [[CrossRef](#)]
17. Ling, Y.; Li, Y.; Xiang, J. Load Support by Droop-Controlled Distributed Generations. *IEEE Trans. Ind. Electron.* **2021**, *68*, 8345–8355. [[CrossRef](#)]
18. Lu, X.; Wang, J.; Guerrero, J.M.; Zhao, D. Virtual-Impedance-Based Fault Current Limiters for Inverter Dominated AC Microgrids. *IEEE Trans. Smart Grid* **2018**, *9*, 1599–1612. [[CrossRef](#)]
19. Meng, X.; Liu, J.; Liu, Z. A Generalized Droop Control for Grid-Supporting Inverter Based on Comparison between Traditional Droop Control and Virtual Synchronous Generator Control. *IEEE Trans. Power Electron.* **2019**, *34*, 5416–5438. [[CrossRef](#)]
20. Jiang, Y.; Pates, R.; Mallada, E. Dynamic Droop Control in Low-Inertia Power Systems. *IEEE Trans. Autom. Control.* **2021**, *66*, 3518–3533. [[CrossRef](#)]
21. Vijay, A.S.; Parth, N.; Doolla, S.; Chandorkar, M.C. An Adaptive Virtual Impedance Control for Improving Power Sharing among Inverters in Islanded AC Microgrids. *IEEE Trans. Smart Grid* **2021**, *12*, 2991–3003. [[CrossRef](#)]
22. Keyvani-Boroujeni, B.; Fani, B.; Shahgholian, G.; Alhelou, H.H. Virtual Impedance-Based Droop Control Scheme to Avoid Power Quality and Stability Problems in VSI-Dominated Microgrids. *IEEE Access* **2021**, *9*, 144999–145011. [[CrossRef](#)]
23. Buraimoh, E.; Davidson, I.E. Fault Ride-Through Analysis of Current- and Voltage-Source Models of Grid Supporting Inverter-Based Microgrid. *IEEE Can. J. Electr. Comput. Eng.* **2021**, *44*, 189–198. [[CrossRef](#)]
24. Rocabert, J.; Luna, A.; Blaabjerg, F.; Rodriguez, P. Control of Power Electronic Converters in AC Microgrid. *IEEE Trans. Power Electron.* **2012**, *27*, 329–355. [[CrossRef](#)]
25. An, R.; Liu, Z.; Liu, J. Successive-Approximation-Based Virtual Impedance Tuning Method for Accurate Reactive Power Sharing in Islanded Microgrids. *IEEE Trans. Power Electron.* **2021**, *36*, 87–102. [[CrossRef](#)]
26. Liu, B.; Wu, T.; Liu, Z.; Liu, J. A Small-AC-Signal Injection-Based Decentralized Secondary Frequency Control for Droop-Controlled Islanded Microgrids. *IEEE Trans. Power Electron.* **2020**, *35*, 11634–11651. [[CrossRef](#)]
27. Tarrasó, A.; Lai, N.B.; Verdugo, C.; Member, S.; Candela, J.I.; Rodriguez, P. Design of Controller for Virtual Synchronous Power Plant. *IEEE Trans. Ind. Appl.* **2021**, *57*, 4033–4041. [[CrossRef](#)]
28. Rouzbehi, K.; Miranian, A.; Candela, J.I.; Luna, A.; Rodriguez, P. A Generalized Voltage Droop Strategy for Control of Multiterminal DC Grids. *IEEE Trans. Ind. Appl.* **2015**, *51*, 607–618. [[CrossRef](#)]
29. Ahmadi, S.; Shokoohi, S.; Bevrani, H. A Fuzzy Logic-Based Droop Control for Simultaneous Voltage and Frequency Regulation in an AC Microgrid. *Int. J. Electr. Power Energy Syst.* **2015**, *64*, 148–155. [[CrossRef](#)]
30. Braitor, A.C.; Konstantopoulos, G.C.; Kadiramanathan, V. Current-Limiting Droop Control Design and Stability Analysis for Paralleled Boost Converters in DC Microgrids. *IEEE Trans. Control Syst. Technol.* **2021**, *29*, 385–394. [[CrossRef](#)]
31. Paspatis, A.G.; Konstantopoulos, G.C.; Guerrero, J.M. Enhanced Current-Limiting Droop Controller for Grid-Connected Inverters to Guarantee Stability and Maximize Power Injection under Grid Faults. *IEEE Trans. Control Syst. Technol.* **2021**, *29*, 841–849. [[CrossRef](#)]

32. Li, Z.; Chan, K.W.; Hu, J.; Guerrero, J.M. Adaptive Droop Control Using Adaptive Virtual Impedance for Microgrids with Variable PV Outputs and Load Demands. *IEEE Trans. Ind. Electron.* **2021**, *68*, 9630–9640. [[CrossRef](#)]
33. Chen, J.; Yue, D.; Dou, C.; Chen, L.; Weng, S.; Li, Y. A Virtual Complex Impedance Based P-V Droop Method for Parallel-Connected Inverters in Low-Voltage AC Microgrids. *IEEE Trans. Ind. Inform.* **2021**, *17*, 1763–1773. [[CrossRef](#)]
34. Tang, M.; Liu, B.; Zhou, Z.; Li, L.Q. Design and Convergence Analysis of an Improved Droop Controller with Adaptive Virtual Impedance. *IEEE Access* **2021**, *9*, 128809–128816. [[CrossRef](#)]
35. Deng, W.; Dai, N.Y.; Lao, K.W.; Guerrero, J.M. A Virtual-Impedance Droop Control for Accurate Active Power Control and Reactive Power Sharing Using Capacitive-Coupling Inverters. *IEEE Trans. Ind. Appl.* **2020**, *56*, 6722–6733. [[CrossRef](#)]